Editors' Suggestion

Voltage-time dilemma and stochastic threshold-voltage variation in pure-silver atomic switches

Anna Nyáry,[1,2,†] Zoltán Balogh,[1,2,†] Máté Vigh,[1] Botond Sánta,[1,2] László Pósa,[1,3] and András Halbritter[1,2,*]

[1] *Department of Physics, Institute of Physics, Budapest University of Technology and Economics (BME), Műegyetem rkp. 3., Budapest H-1111, Hungary*

[2] *HUN-REN-BME Condensed Matter Research Group, Műegyetem rkp. 3., Budapest H-1111, Hungary*

[3] *Institute of Technical Physics and Materials Science, HUN-REN Centre for Energy Research, Konkoly-Thege M. út 29-33., Budapest H-1121, Hungary*

(Received 11 July 2023; accepted 15 December 2023; published 17 January 2024)

The formation and dissolution of silver nanowires plays a fundamental role in a broad range of resistive-switching devices, which fundamentally rely on the electrochemical-metallization phenomenon. It has been shown that resistive switching may also appear in pure metallic nanowires lacking any silver-ion-hosting embedding environment but this pure atomic switching mechanism differs fundamentally from the conventional electrochemical-metallization-based resistive switching. To facilitate the quantitative description of the former phenomenon, we investigate a broad range of Ag atomic junctions, with a special focus on the frequency dependence and the fundamentally stochastic cycle-to-cycle variation of the switching-threshold voltage. These devices are established in an ultrahigh-purity environment in which electrochemical metallization can be excluded. The measured characteristics are successfully described by a vibrational-pumping model, yielding consistent predictions for the weak frequency dependence and the large variance of the switching-threshold voltage. We also demonstrate that electrochemical-metallization-based resistive switching and pure atomic switching may appear in the same device structure and therefore the proper understanding of the pure atomic switching mechanism has a very relevant importance in silver-based electrochemical-metallization cells.

DOI: 10.1103/PhysRevApplied.21.014027

I. INTRODUCTION

In the past decade, the resistive-switching phenomenon has been established in various material systems, promoting novel, energy-efficient, fast, and compact technologies in the fields of nonvolatile data storage, in-memory computing, or the hardware implementation of artificial neural networks [1–5]. A distinguished group of resistive-switching memory devices relies on the voltage-controlled dissolution of metallic cations in an insulating matrix, resulting in the formation or destruction of ultrasmall close to atomic sized metallic filaments between the contacting electrodes [6–16]. In such structures, voltage-induced cation migration and electrochemical metallization (ECM) play key roles in the programming of the devices, i.e., in the adjustment of the filament diameter.

Recently, it has been shown that resistive switching can also be induced in completely pure metallic wires, which lack any ion-hosting embedding environment [17–21]. In this case, reversible voltage-induced atomic rearrangements are observed in nanojunctions where the size of the wire bottleneck approaches the ultimate single-atom regime. These atomic rearrangements are reflected by discrete jumps in the conductance state of the metallic nanowire. Such *pure atomic switching* (PAS) has been realized in various pure metallic systems, including Au, Cu, Al, and Pb nanowires [17–21].

In this paper, we argue that the PAS phenomenon is not restricted to pure metallic nanowires and that it may also become important in conventional electrochemical-metallization cells, once atomic size scales are reached. From this reason, it is of fundamental importance to explore the differences between PAS- and ECM-type switching (ECMS) and to understand the physical mechanisms governing the former phenomenon. Although a broad range of material systems exhibit ECMS, silver plays a prominent role as an active material in such devices. To this end, we compare the PAS and ECMS characteristics in silver-based platforms and in order to achieve an unquestionable distinction between the two types of phenomena, the PAS phenomenon is explored in

*halbritter.andras@ttk.bme.hu; author to whom correspondence should be addressed.

†A.N. and Z.B. contributed equally to this work.

ultrapure-silver nanowires, where electrochemical metallization can be excluded. Our analysis puts a special emphasis on the experimental investigation of the frequency dependence, as well as the fundamentally stochastic variation of the switching-threshold voltage, both being characteristic of the PAS phenomenon. Finally, we propose a vibrational-pumping model of the PAS process, which consistently describes the observed phenomena.

II. RESULTS AND DISCUSSION

A. Comparison of PAS and ECMS characteristics

In our previous work, scanning-tunneling-microscopy point-contact measurements on sulphurized thin Ag samples have already exhibited fundamentally different resistive-switching characteristics in ultrasmall atomic junctions compared to the somewhat larger nanoscale point contacts [22]. Here, we present another example of this phenomenon, relying on our $Ag/Ag_2S/Ag$ nanofabricated memristive devices [11] [see the SEM image of the device in the inset of Fig. 1(a) and more details in the caption]. In the higher-conductance regime, these nanojunctions have been shown to exhibit conventional ECMS characteristics (see our previous results in Ref. [11]), which is also illustrated by another data set with 20 reproducible ECMS switching cycles in Fig. 1(a). In Fig. 1(b), however, we demonstrate a room-temperature resistive switching of a fundamentally different nature, closely resembling the PAS-type characteristics of other metallic species [18–20]. These switching characteristics have been observed using the same $Ag/Ag_2S/Ag$ nanofabricated memristive devices, by driving them to the conductance range of the $G_0 = 2e^2/h$ conductance quantum unit. Whereas the ECM-type switching of the larger junctions [Fig. 1(a)] exhibits a gradual and basically reproducible transition between the high and low-conductance states (HCS and LCS, respectively) at a few-hundred-millivolts switching-threshold-voltage characteristic of the Ag_2S resistive-switching system [23, 24], Fig. 1(b) exhibits a jumplike switching between two discrete atomic arrangements at an order-of-magnitude-higher but fundamentally stochastic threshold voltage. In this illustrative measurement, however, the Ag junction has been deliberately sulphurized, i.e., pure metallic conditions have not been satisfied, and the role of the silver-sulfide matrix in the atomic sized switching process of Fig. 1(b) remains unclarified.

Here, our primary goal is the investigation and deeper understanding of the PAS mechanism in an environment, in which any other types of resistive-switching mechanisms can be ruled out. To this end, we have performed our measurements using a cryogenic temperature (4.2-K) notched-wire mechanically controllable break-junction (MCBJ) setup, where atomic sized nanowires are established by the controlled mechanical rupture of a high-purity metallic wire using a three-point-bending

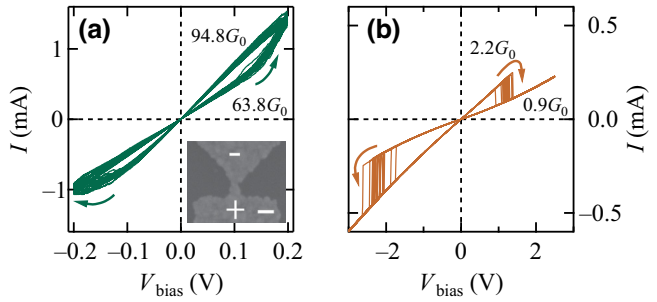

FIG. 1. The coexistence of ECMS and PAS characteristics in a nanofabricated $Ag/Ag_2S/Ag$ memristive device. The current-voltage characteristics of reproducible switchings measured in the (a) nanoscale and (b) atomic scale regimes, exhibiting (a) ECMS and (b) PAS characteristics. The legends demonstrate the average HCS and LCS conductances. These $Ag/Ag_2S/Ag$ samples are fabricated by electron-beam lithography, establishing an approximately 45-nm-thick and approximately 100-nm-wide Ag nanobridge. This is further narrowed by a controlled electromigration protocol [22,25]. The resulting nanojunction is exposed to vaporized sulfur to create the electrochemical-metallization switching medium between the Ag electrodes. The inset of (a) shows a scanning-electron-microscopy picture of the constriction in the sample, the scale bar indicating a distance of 200 nm. The $\pm$ signs indicate the voltage polarity on the junction at positive biasing. It is to be noted that these devices lack compositional asymmetry (Ag electrodes contact the junction from both sides) and therefore the well-defined switching polarity in the case of ECMS is attributed to the geometrical asymmetry of the junction. In case of PAS, the switching polarity varies according to the geometry of the actual atomic arrangement of the junction.

geometry [see Fig. 2(d)]. The *in situ* rupture in the cryogenic vacuum excludes the oxidation and/or contamination of the nanowire, while the MCBJ arrangements grants an ultrahigh mechanical stability. The current-voltage ($I(V)$) characteristics of the thus-obtained ultrahigh-purity silver atomic wires readily exhibit typical PAS behavior [Figs. 2(a)–2(c)], resembling the PAS curves of other [18–20] previously studied but nonsilver pure metallic systems.

Later on, we investigate further properties of the PAS mechanism in Ag atomic wires, including the switching-to-switching and sample-to-sample variation of the V_{thr} switching-threshold voltages as well as the sweep-rate dependence of V_{thr}. We compare these characteristics to the fundamentally different properties of conventional ECM-type resistive-switching traces, relying on the further analysis of our previously measured data on AgI resistive-switching STM point contacts [15], where a significant amount of statistically independent data is available [see the illustration of the AgI point contacts in Fig. 2(e) and the example $I(V)$ curves in Fig. 2(f)]. As a next step, we propose a vibrational-pumping model that describes the observed PAS characteristics remarkably well.

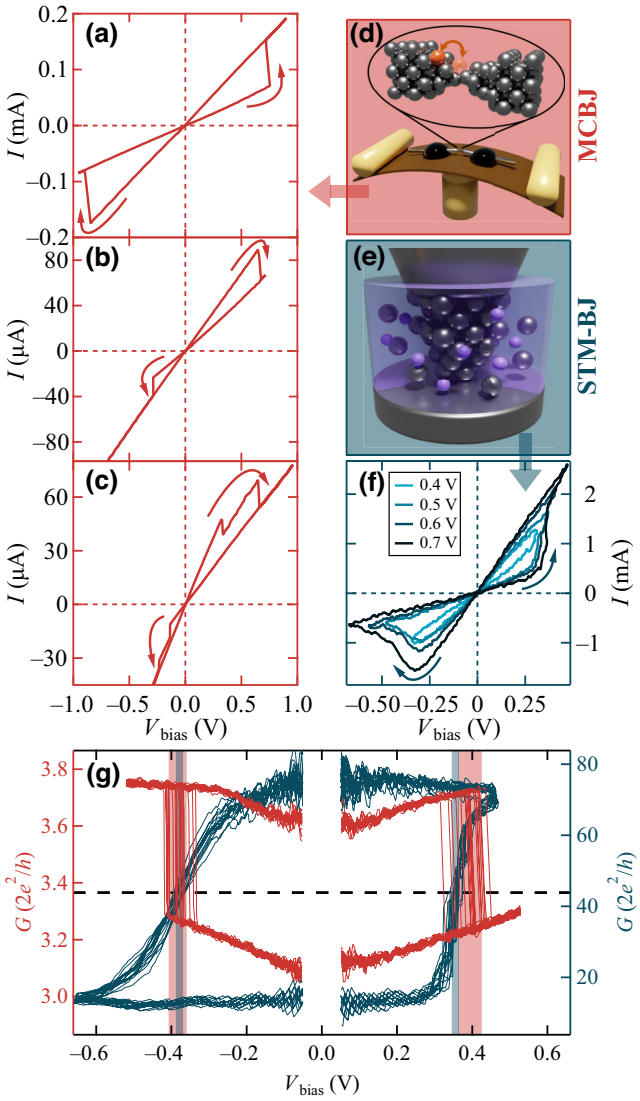

FIG. 2. A comparison of the PAS and ECMS characteristics. (a)–(d) The illustrations exemplify the (a) rather symmetric or (b),(c) highly asymmetric PAS characteristics with a reproducible switching between (a),(b) two or (c) three atomic configurations. The PAS measurements are performed at cryogenic temperature ($T = 4.2$ K) using (d) the MCBJ technique. In this case, a serial resistance of 520 Ω has been applied. (e),(f) As a comparison, ECMS is investigated on AgI thin films using (e) the room-temperature STM break-junction (STM-BJ) technique, exhibiting (f) driving-voltage-amplitude-dependent multilevel programming characteristics. The legends show the amplitudes of the driving triangular voltage signals. Here, a serial resistance of 150 Ω has been applied. (g) A representative example of PAS and ECMS with similar switching-threshold voltages. Here, the conductance versus bias voltage curve is plotted and the black dashed line shows the mean value of the HCS and LCS conductances for the two systems. The switching-threshold voltages and their standard deviations are evaluated at this conductance cut for both the set and reset transitions, yielding $\Delta V_{\mathrm{thr}}^{\mathrm{set}}/\overline{V}_{\mathrm{thr}}^{\mathrm{set}} = -0.062$ and $\Delta V_{\mathrm{thr}}^{\mathrm{reset}}/\overline{V}_{\mathrm{thr}}^{\mathrm{reset}} = 0.078$ for PAS (red); while $\Delta V_{\mathrm{thr}}^{\mathrm{set}}/\overline{V}_{\mathrm{thr}}^{\mathrm{set}} = 0.027$ and $\Delta V_{\mathrm{thr}}^{\mathrm{reset}}/\overline{V}_{\mathrm{thr}}^{\mathrm{reset}} = -0.027$ for ECMS (blue).

The different behavior of PAS and ECMS is already obvious from the switching $I(V)$ curves. (i) PAS displays abrupt jumps between discrete conductance states [Figs. 2(a)–2(c)], corresponding to discrete geometrical configurations of the atomic wire. As a sharp contrast, ECMS is accompanied by a more gradual transition between the HCS and the LCS, as shown in Fig. 2(f). (ii) In the case of ECMS, the analog multilevel programming of the conductance states is a well-known phenomenon. This means that the increase of the driving-voltage amplitude continuously tunes the HCS and LCS conductances and thereby the $G_{\mathrm{HCS}}/G_{\mathrm{LCS}}$ conductance ratio [Fig. 2(f)] [15,24]. In contrast, PAS yields driving-voltage-independent HCS and LCS conductances as long as a further atomic jump, resulting in discrete multilevel states, is not reached [for a PAS with three distinct conductance states, see Fig. 2(c)]. (iii) The switching direction [indicated by arrows in Figs. 2(a)–2(c) and 2(f)] is defined by the material and geometrical asymmetry in the case of ECMS, i.e., the set (LCS → HCS) transition always happens at positive voltage polarity, where the Ag layer is biased positively with respect to the electrochemically inert Pt-Ir tip and, accordingly, the reset (HCS → LCS) transition occurs at negative bias. As a sharp contrast, in the case of PAS, the switching direction is determined by the local atomic sized geometry of the few-atom active region and therefore the switching direction varies from junction to junction.

A further remarkable difference is observed in the cycle-to-cycle variation of the switching, as shown in Fig. 2(g), demonstrating approximately 20 consecutive cycles for an example PAS (red) and an example ECMS (blue), both exhibiting set and reset transitions at similar voltages. Note that in this case, the $G = I/V$ conductance is plotted as a function of the bias voltage and the switching-threshold voltage is identified by the bias voltage, where the $G(V)$ curve crosses the average $((G_{\mathrm{HCS}} + G_{\mathrm{LCS}})/2)$ conductance (black dashed line). It is clear that the ECMS is a basically reproducible process and, accordingly, the standard deviation of the switching-threshold voltage, ΔV_{thr}, is small compared to the average value, $\overline{V}_{\mathrm{thr}}$. In contrast, the switching-threshold voltage shows a broader fundamentally stochastic cycle-to-cycle variation in the case of PAS, yielding significantly higher $\Delta V_{\mathrm{thr}}/\overline{V}_{\mathrm{thr}}$ ratios (for the numerical values, see the caption).

Next, we analyze the device-to-device variation of the threshold voltages. For this, in Fig. 3(a) we plot the mean threshold voltages of set transitions (circles) and reset transitions (squares) for independent measurements of reproducible switchings as a function of the initial conductance state [i.e., the LCS (HCS) in the case of the set (reset) transition] both for PAS (red) and for ECMS (blue). The right panel of Fig. 3(a) shows the corresponding histogram of the threshold voltages. In the figure, the difference between PAS and ECMS is clearly

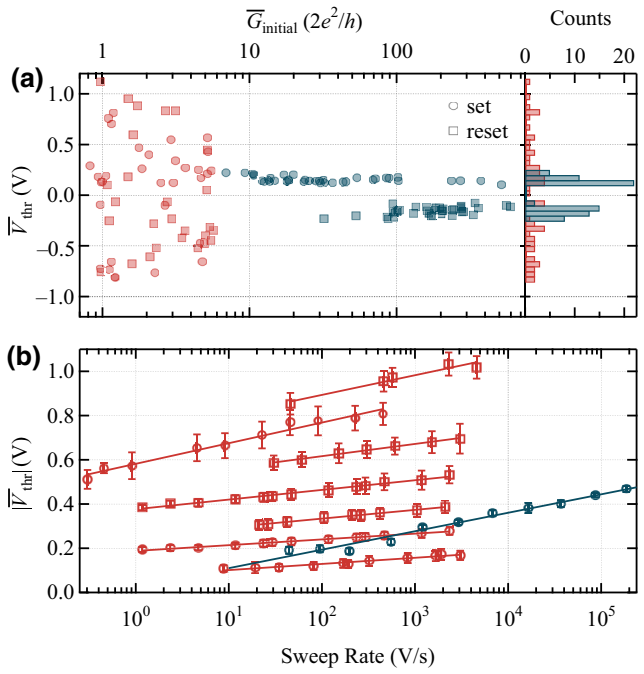

FIG. 3. The device-to-device variation and sweep-rate dependence of the threshold voltage. (a) The set (circle) and reset (square) threshold voltages of several PAS processes (red) and ECMS processes (blue) with various initial conductances. The right panel summarizes the data in a histogram. (b) The sweep-rate dependence of the threshold voltages for representative PAS processes (red) and an ECMS measurement (blue). The error bars represent the cycle-to-cycle standard deviation of V_{thr} for the various measurements, while the lines represent linear fits to the data along linear $\overline{V}_{\mathrm{thr}}$ and logarithmic sweep-rate axes.

distinguishable: the ECMS threshold voltages exhibit well-defined and relatively low values around ± 155 mV, whereas the PAS V_{thr} values show a wide distribution exhibiting order-of-magnitude device-to-device differences up to ± 1 V. Furthermore, this upper limit seems to be related to the limited stability of the break-junction arrangement at even higher voltage drives, whereas the more stable nanofabricated samples may also exhibit even higher thresholds [see Fig. 1(b)]. Moreover, we can again observe clear confirmation about the switching direction being well defined for ECMS (the set transition occurs at positive voltage) and stochastic for PAS. It can also be noted that the relation of the set and reset voltages also shows a broad variation in the case of PAS, with some curves exhibiting similar set and reset voltages [see Fig. 2(a)] while other junctions show extremely different set and reset voltages [see Fig. 2(b)].

So far, we have investigated the switching characteristics at specific frequencies but now we turn to the time dependence and aim to explore the so-called voltage-time dilemma, which is a well-known phenomenon in memristive systems [15,24,26] and can be summarized as the exponential acceleration of the switching time while linearly increasing the applied voltage. Figure 3(b) depicts the absolute value of the threshold voltage as the function of the sweep rate for selected representative atomic switchings in different ranges of threshold voltages (red symbols). A clear exponential dependence (i.e., a linear trend on a linear-logarithmic scale) is visible; however, the variation of the threshold voltage with the sweep rate is rather small: typically $\overline{V}_{\mathrm{thr}}$ increases by 10% as the sweep rate increases by a decade [for a quantitative slope analysis, see the circles in Fig. 4(d)]. As a comparison, the Ag/AgI/(Pt-Ir) ECMS system [blue curve in Fig. 3(b)] shows a more than twice as large relative variation of V_{thr} in the same sweep-rate interval, whereas there are also examples of an Ag-based ECMS exhibiting an approximately 100% relative increase of the threshold voltage within one decade along the temporal axis [27–29]. We also note that memristive switching experiments have already demonstrated ultrafast measurements going down to switching times of 10 ps at the present instrumental resolution limit [15,30–33], where the time-resolved tracking of thermal relaxation processes is already possible [33]. Here, this type of time-resolved insight into the PAS phenomenon is not yet available, being limited by the low bandwidth of our conventional low-temperature break-junction setup.

B. Theoretical model of atomic switching and numerical simulations

In the following, we present a theoretical model with the goal of describing the PAS, with special emphasis on the large stochastic cycle-to-cycle variation of the threshold voltage and the rather weak dependence of the threshold voltage on the sweep rate. Considering a conventional electromigration picture, the PAS could be related to current-induced forces, such that the current density is the relevant driving parameter of the switching [34]. In that case, junctions with different diameters should perform atomic switching at similar current densities. This picture, however, is not consistent with the experiments of Ref. [21], where atomic junction instabilities have been studied for various materials and junction sizes. Instead, Ref. [21] has described the switching phenomenon by the pumping of particular phonon modes, also considering the contact destabilization by *runaway phonon modes* due to nonconservative forces. In addition, Ref. [35] has proposed to estimate the material-dependent threshold voltages based on first-principles calculation of the current-induced tensile strength in ballistic conductors, yielding the same sequence of threshold voltages as experimentally observed in Ref. [21]. Here, we apply a similar but simpler approach to the phonon-pumping model of Ref. [21] but solely relying on a conventional vibrational-pumping model [36,37], i.e., excluding nonconservative forces and current-induced bond weakening. We demonstrate that

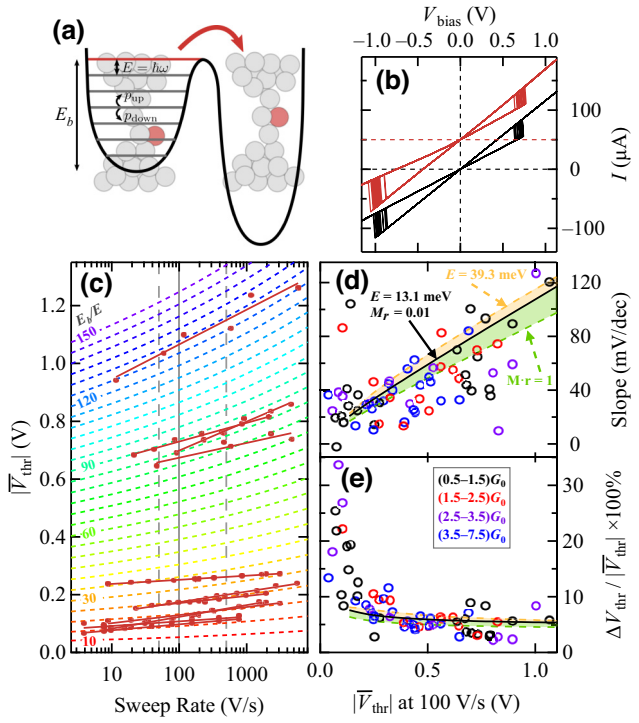

FIG. 4. A comparison of the measured and simulated switching characteristics. (a) An illustration of the model energy landscape and a sketch naively illustrating the switching process. (b) A comparison of 20 measured (red) current-voltage characteristics and simulated (black) switching characteristics. The measured $I(V)$ curve is vertically shifted for clarity. (c) The measured (red dots) and simulated (colored dashed lines) sweep-rate dependence of the threshold voltage. Both the simulations and the measurements are related to the case of a single conductance channel (i.e., junctions with an initial conductance of $G = 1 \pm 0.15\ G_0$ are selected in the case of the measurements). (d) The slope of the simulated and measured $\overline{V}_{thr}$ versus log(sweep rate) curves as a function of $\overline{V}_{thr}$ at a 100 V/s sweep rate. The slope is evaluated in the 50–500 V/s interval [gray dashed lines in (c)]. (e) The cycle-to-cycle standard deviation of the switching-threshold voltage normalized to $\overline{V}_{thr}$ as a function of the mean threshold voltage evaluated at 100 V/s. In (d) and (e), the colored circles represent the measured data according to the color code in the legend of (e). The black lines represent the simulated data using $E = 13.1$ meV, $Mr = 0.01$, and $\gamma = 3$. The yellow and green dashed lines, respectively, represent the variation of the simulated results by changing a single parameter (i.e., using $E = 39.3$ meV or $Mr = 1$, respectively) and leaving all the other parameters unchanged.

this simplified model is already sufficient to describe the sweep-rate dependence and the cycle-to-cycle variation of the threshold voltage.

The basic idea of the model is presented in Fig. 4(a): two metastable junction configurations are considered, which are described by a double-well potential. At a certain voltage, the final state is considered as the more stable (lower-energy) configuration. However, an energy barrier of E_b must be reached for the switching. For this, the electrons cannot transfer enough energy to the switching atom within a single scattering process; however, multiple scattering events may *pump* the proper vibrational mode, described by energy quanta $E = \hbar\omega$. Our model describes the voltage-induced evolution of the vibrational energy states as a random walk along the energy ladder, described by $p_{up}(\Delta t)$ and $p_{down}(\Delta t)$ upward and downward jump probabilities within a time step Δt. These probabilities are taken from the zero-temperature limit of the single-vibrational-level model of Ref. 37 using M open channels (for more details, see the Supplemental Material [38]). This yields

$$p_{up}(\Delta t) = \frac{2Mr\Delta t}{h}(n+1)(eV - E)$$

and

$$p_{down}(\Delta t) = \frac{2Mr\Delta t}{h} n\,(eV + (3+4\gamma)E)$$

for the energy absorption from the electrons or the energy emission from the vibrational mode to the electrons, respectively. Here, V is the bias voltage, h is Planck's constant, n is the occupation number of the vibrational mode, and r describes the ratio of the electrons interacting with the vibrational mode, which is approximated by the $r = 0.01$ typical value according to the fitting of the point-contact spectroscopy measurements on an Au atomic contact in Ref. [37,39]. The $\gamma = \gamma_d/\gamma_{eh}$ parameter describes the ratio of the electron-phonon coupling strength (γ_{eh}) to the phonon-phonon damping parameter (γ_d), as described in more detail in the Supplemental Material [38]. In our simulations, $\gamma = 3$ is used, based on the value determined for a gold wire in the work of Paulsson *et al.* [37,39]. The value of the phonon energy quantum is estimated to be $E = 13.1$ meV in the Ag atomic wire based on the homology of forces [40] applied to the simulated mean value of the mean phonon energy quantum of Cu atomic wires [21]. According to the highly open conductance channels of Ag atomic wires, the number of open channels is estimated from the G conductance as $M = \text{round}(G/G_0)$. The model is invariant for the actual value of Δt; however, the time step should be sufficiently small to satisfy the $p_{up}(\Delta t) + p_{down}(\Delta t) < 1$ condition for the investigated n and V values.

In our simulation, the voltage is increased with a predefined sweep rate and, meanwhile, a random walk along the energy ladder is considered according to the above rules (for more details, see the Supplemental Material [38]). The switching happens at the voltage at which the E_b barrier energy is reached for the first time. At this point, the system switches to the other, more stable, configuration, from which no back switching is considered as the voltage is further increased. The simulation delivers the probability density function of the voltages needed to reach the

E_b energy barrier at a given sweep rate. From this, both the average and the standard deviation of the switching-threshold voltage can be determined at an arbitrary sweep rate.

We emphasize that our approach applies fixed physically motivated model parameters and that the E_b barrier energy is the only free parameter, which is rather directly related to the V_{thr} switching voltage. On the other hand, the energy landscape [Fig. 4(a)] of the system is considered to be modified by the applied voltage, presumably yielding a decrease of E_b with increasing voltage. Furthermore, the energetically more stable atomic configurations should be interchanged at reversed voltage polarity. These processes are not modeled in our simulation. We argue, however, that at low enough voltages, where the probability of reaching the barrier energy is negligible, the actual value of E_b is insignificant. Therefore, we consider E_b as the characteristic barrier height in the voltage interval, where the switching has a reasonable probability, i.e., in the voltage region, where the experimentally measured V_{thr} values scatter. We also emphasize, that the huge sample-to-sample variation of V_{thr} in Fig. 3(a) implies a very broad variation of the possible atomic arrangements (and possible barrier energies). Accordingly, we cannot propose any specific atomic arrangements in our model: the sketches in Fig. 4(a) are only naive illustrations.

C. Comparison of the experimental data and the model calculations

Figure 4(b) compares measured (red) and simulated (black) PAS $I(V)$ curves both including 20 switching cycles. In the simulation, the HCS and LCS conductances and the sweep rate are set according to the measured $I(V)$ curve and the E_b^{set} and E_b^{reset} barrier energies are adjusted such that the average switching voltages of the measurement are reproduced. This simulated stochastic cycle-to-cycle variation of the switching voltage resembles that of the measured data very closely.

To obtain a further comparison, we investigate the sweep-rate dependence of the switching [Fig. 4(c)]. The simulated mean threshold voltages for $M = 1$, $r = 0.01$, $E = 13.1$ meV, and $\gamma = 3$ are plotted as a function of the sweep rate in Fig. 4(c) for various E_b energy barriers by colored dashed lines. As a comparison, the sweep-rate-dependent measured mean threshold voltages of PAS states with an initial conductance of $G = 1 \pm 0.15\ G_0$ are shown by red circles. The red lines represent linear fits to the data along linear V_{thr} and logarithmic sweep-rate axes. The slope of these fits very closely resembles the slopes of the simulated curves, with both exhibiting an increasing slope with increasing V_{thr}. Note that this comparison with the simulations allows the estimation of the energy barrier required for the atomic switching in a particular experiment (see the colored E_b/E values on the simulated curves).

For a more quantitative analysis, Fig. 4(d) compares the threshold-voltage dependencies of the measured and simulated slopes, i.e., the change of $\overline{V}_{thr}$ along the one-decade change of the sweep rate between the gray dashed lines in Fig. 4(c). Note that in Fig. 4(b), the presented simulations and experiments have been restricted to the single-channel ($M = 1$) situation. Figure 4(d), however, shows the measured slopes (circles) for all the sweep-rate-dependent measurements as a function of $\overline{V}_{thr}$ encoding the conductance range of the initial state with colors. This color coding does not exhibit any obvious conductance dependence of the measured slope values. The $\overline{V}_{thr}$-dependent simulated slopes at $M = 1$, $r = 0.01$, and $E = 13.1$ meV are plotted by a black line. The colored dashed lines illustrate the sensitivity of the model to the parameters. A threefold increase of E (yellow dashed line) as well as a 100-fold increase of M or r (i.e., the 100-fold increase of Mr as demonstrated by the green dashed line) yield a very modest variation of the simulated slope values (for a more detailed investigation of the dependence on the model parameters, see the Supplemental Material [38]). To conclude this analysis: in spite of the scattering of the experimental data, the simulated and the measured slope values cover the same slope range, exhibiting a very similar $\overline{V}_{thr}$ dependence. Furthermore, the simulated slope versus $\overline{V}_{thr}$ curve is rather insensitive to the model parameters; in particular, the junction conductance ($G \sim M$) does not influence the slope values significantly. On the other hand, we emphasize that our simplified model does not capture many details of the actual switching process; in particular, the obvious voltage-dependent deformation of the potential landscape as the switching is approached, as well as the current-induced or nonconservative forces acting on the switching atom [41,42]. Furthermore, the role of these aspects is expected to be different for each individual junction arrangement, which might explain the broad variance of the experimental data points around the general tendency predicted by our simplified model.

Next, we investigate the $\overline{V}_{thr}$ dependence of the cycle-to-cycle standard deviation of the threshold voltages, ΔV_{thr} normalized to $\overline{V}_{thr}$. The colored circles (solid and dashed lines) are related to the same experimental (simulational) data as in Fig. 4(d), using the same color coding. This analysis also shows a very good correspondence between the experiment and the simulation, exhibiting a rather constant $\Delta V_{thr}/\overline{V}_{thr} \approx 5\%$ value. A significant deviation from this is only observed at low threshold voltages. In this range, a few phonon energy quanta are sufficient to reach the barrier, i.e., the model calculation is expected to be less reliable. Furthermore, the repeated cycling may also introduce slight variations in the two atomic arrangements, even if the conductances of the two states seem to be similar in the subsequent cycles. The latter issue may introduce

an additional cycle-to-cycle variance of the threshold voltage, which may also explain the deviation from the model curves, especially in the low-threshold region, where the normalization to the low V_{thr} magnifies a small excess value of ΔV_{thr} (for more details, see the Supplemental Material [38]).

III. CONCLUSIONS

In conclusion, we have performed a quantitative analysis of the pure atomic switching phenomenon in cryogenic temperature silver break junctions, where electrochemical-metallization-type resistive-switching mechanisms can be excluded. We have demonstrated that PAS exhibits fundamentally different characteristics compared to conventional ECM-type resistive-switching mechanisms: in particular, the switching-threshold voltage exhibits a huge device-to-device variation—a large, fundamentally stochastic, cycle-to-cycle variation—however, it depends rather weakly on the driving frequency. All these phenomena have been successfully described by a simple model relying on the pumping of a single vibrational mode by the electrons scattering at the device bottleneck. By simulating the random walk along the energy ladder of the vibrational mode and identifying the switching mechanism by the first reaching the proper barrier energy, we could provide a consistent model of the experimental observations, quantitatively describing the weak frequency dependence of the switching-threshold voltage, as well as its stochastic cycle-to-cycle variation.

Our above measurements on undoubtedly pure Ag atomic wires very much resemble the switching characteristics of sulphurized silver devices driven to the range of the conductance quantum unit, i.e., Ag_2S resistive-switching units with a few atoms in the active volume (see Fig. 1(b) and Ref. [22]). This comparison implies that in the latter case, the conventional ECMS is replaced by a fundamentally different physical mechanism, where the role of the Ag ions in the embedding Ag_2S environment become irrelevant and, rather, the PAS phenomenon characteristic of atomic sized pure metallic nanowires becomes the dominant process. This analysis raises the possible emergence of the PAS phenomenon in a wider range of atomic sized ECM-type resistive-switching systems, highlighting the need for the proper characterization and understanding of the PAS phenomenon.

ACKNOWLEDGMENTS

This research was supported by the Ministry of Culture and Innovation, the National Research, Development, and Innovation Office (NKFI) within the Quantum Information National Laboratory of Hungary (Grant No. 2022–2.1.1-NL-2022-00004) and the NKFI Grants No. K128534, No. K143169, and No. K143282. Z.B. (L.P.) acknowledges the support of the BO/00691/21 (BO/00746/21) Bolyai János Research Scholarship of the Hungarian Academy of Sciences and the ÚNKP-22-5-BME-288 (ÚNKP-22-5-BME-329) New National Excellence Program of the Ministry for Innovation and Technology from the National Research, Development, and Innovation Fund. The cryogenic measurements were supported by the helium-liquefaction plant of the BME (VEKOP 2.3.3-15-2017-00015) Competitive Central-Hungary Operative Program from the European Regional Development Fund.

The measurements on Ag nanowires and the evaluation of the experimental data were carried out by A.N. The modeling and the simulations were performed by Z.B. with fundamental contributions from A.H., A.N., and M.V. The measurements on the Ag/AgI/(Pt-Ir) samples were performed by B.S. and the measurements on the $Ag/Ag_2S/Ag$ samples were performed by L.P. The work was supervised by A.H. and Z.B. The manuscript was written by A.H., A.N., and Z.B.

[1] J. J. Yang, D. B. Strukov, and D. R. Stewart, Memristive devices for computing, Nat. Nanotechnol. **8**, 13 (2013).
[2] D. Ielmini and S. Ambrogio, Emerging neuromorphic devices, Nanotechnology **31**, 092001 (2020).
[3] Z. Wang, H. Wu, G. W. Burr, C. S. Hwang, K. L. Wang, Q. Xia, and J. J. Yang, Resistive switching materials for information processing, Nat. Rev. Mater. **5**, 173 (2020).
[4] S. H. Lee, X. Zhu, and W. D. Lu, Nanoscale resistive switching devices for memory and computing applications, Nano Res. **13**, 1228 (2020).
[5] Y. Li and K.-W. Ang, Hardware implementation of neuromorphic computing using large-scale memristor crossbar arrays, Adv. Intell. Syst. **3**, 2000137 (2021).
[6] K. Terabe, T. Hasegawa, T. Nakayama, and M. Aono, Quantized conductance atomic switch, Nature **433**, 47 (2005).
[7] I. Valov, R. Waser, J. R. Jameson, and M. N. Kozicki, Electrochemical metallization memories—fundamentals, applications, prospects, Nanotechnology **22**, 254003 (2011).
[8] I. Valov, I. Sapezanskaia, A. Nayak, T. Tsuruoka, T. Bredow, T. Hasegawa, G. Staikov, M. Aono, and R. Waser, Atomically controlled electrochemical nucleation at superionic solid electrolyte surfaces, Nat. Mater. **11**, 530 (2012).
[9] Y. Yang, P. Gao, S. Gaba, T. Chang, X. Pan, and W. Lu, Observation of conducting filament growth in nanoscale resistive memories, Nat. Commun. **3**, 732 (2012).
[10] A. Geresdi, M. Csontos, A. Gubicza, A. Halbritter, and G. Mihály, A fast operation of nanometer-scale metallic memristors: Highly transparent conductance channels in Ag_2S devices, Nanoscale **6**, 2613 (2014).
[11] A. Gubicza, D. Z. Manrique, L. Pósa, C. J. Lambert, G. Mihály, M. Csontos, and A. Halbritter, Asymmetry-induced resistive switching in Ag-Ag_2S-Ag memristors enabling a simplified atomic-scale memory design, Sci. Rep. **6**, 30775 (2016).
[12] S. Choi, S. H. Tan, Z. Li, Y. Kim, C. Choi, P. Y. Chen, H. Yeon, S. Yu, and J. Kim, SiGe epitaxial

memory for neuromorphic computing with reproducible high performance based on engineered dislocations, Nat. Mater. **17**, 335 (2018).

[13] Z. Wang, M. Rao, R. Midya, S. Joshi, H. Jiang, P. Lin, W. Song, S. Asapu, Y. Zhuo, C. Li, H. Wu, Q. Xia, and J. J. Yang, Threshold switching of Ag or Cu in dielectrics: Materials, mechanism, and applications, Adv. Funct. Mater. **28**, 1704862 (2018).

[14] B. Sánta, Z. Balogh, A. Gubicza, L. Pósa, D. Krisztián, G. Mihály, M. Csontos, and A. Halbritter, Universal $1/f$ type current noise of Ag filaments in redox-based memristive nanojunctions, Nanoscale **11**, 4719 (2019).

[15] B. Sánta, D. Molnár, P. Haiber, A. Gubicza, E. Szilágyi, Z. Zolnai, A. Halbritter, and M. Csontos, Nanosecond resistive switching in Ag/AgI/PtIr nanojunctions, Beilstein J. Nanotechnol. **11**, 92 (2020).

[16] J. J. Wagenaar, M. Morales-Masis, and J. M. Van Ruitenbeek, Observing quantized conductance steps in silver sulfide: Two parallel resistive switching mechanisms, J. Appl. Phys. **111**, 014302 (2012).

[17] C. A. Martin, R. H. Smit, H. S. Van Der Zant, and J. M. Van Ruitenbeek, A nanoelectromechanical single-atom switch, Nano Lett. **9**, 2940 (2009).

[18] C. Schirm, M. Matt, F. Pauly, J. C. Cuevas, P. Nielaba, and E. Scheer, A current-driven single-atom memory, Nat. Nanotechnol. **8**, 645 (2013).

[19] Q. Wang, R. Liu, D. Xiang, M. Sun, Z. Zhao, L. Sun, T. Mei, P. Wu, H. Liu, X. Guo, Z.-L. Li, and T. Lee, Single-atom switches and single-atom gaps using stretched metal nanowires, ACS Nano **10**, 9695 (2016).

[20] K. Yoshida and K. Hirakawa, Stochastic resonance in bistable atomic switches, Nanotechnology **28**, 125205 (2017).

[21] M. Ring, D. Weber, P. Haiber, F. Pauly, P. Nielaba, and E. Scheer, Voltage-induced rearrangements in atomic-size contacts, Nano Lett. **20**, 5773 (2020).

[22] A. Geresdi, A. Halbritter, A. Gyenis, P. Makk, and G. Mihály, From stochastic single atomic switch to nanoscale resistive memory device, Nanoscale **3**, 1504 (2010).

[23] A. Gubicza, M. Csontos, A. Halbritter, and G. Mihály, Resistive switching in metallic Ag_2S memristors due to a local overheating induced phase transition, Nanoscale **7**, 11248 (2015).

[24] A. Gubicza, M. Csontos, A. Halbritter, and G. Mihály, Non-exponential resistive switching in Ag_2S memristors: A key to nanometer-scale non-volatile memory devices, Nanoscale **7**, 4394 (2015).

[25] C. Nef, L. Pósa, P. Makk, W. Fu, A. Halbritter, C. Schönenberger, and M. Calame, High-yield fabrication of nm-size gaps in monolayer CVD graphene, Nanoscale **6**, 7249 (2014).

[26] R. Waser, R. Dittmann, C. Staikov, and K. Szot, Redox-based resistive switching memories—nanoionic mechanisms, prospects, and challenges, Adv. Mater. **21**, 2632 (2009).

[27] S. Tappertzhofen, I. Valov, and R. Waser, Quantum conductance and switching kinetics of AgI-based microcrossbar cells, Nanotechnology **23**, 145703 (2012).

[28] J. van den Hurk, V. Havel, E. Linn, R. Waser, and I. Valov, Ag/GeS_x/Pt-based complementary resistive switches for hybrid CMOS/nanoelectronic logic and memory architectures, Sci. Rep. **3**, 2856 (2013).

[29] W. Chen, S. Tappertzhofen, H. J. Barnaby, and M. N. Kozicki, SiO_2 based conductive bridging random access memory, J. Electroceram. **39**, 109 (2017).

[30] A. C. Torrezan, J. P. Strachan, G. Medeiros-Ribeiro, and R. S. Williams, Sub-nanosecond switching of a tantalum oxide memristor, Nanotechnology **22**, 485203 (2011).

[31] M. von Witzleben, T. Hennen, A. Kindsmüller, S. Menzel, R. Waser, and U. Böttger, Study of the SET switching event of VCM-based memories on a picosecond timescale, J. Appl. Phys. **127**, 204501 (2020).

[32] M. von Witzleben, S. Wiefels, A. Kindsmüller, P. Stasner, F. Berg, F. Cüppers, S. Hoffmann-Eifert, R. Waser, S. Menzel, and U. Böttger, Intrinsic RESET speed limit of valence change memories, ACS Appl. Electron. Mater. **3**, 5563 (2021).

[33] M. Csontos, Y. Horst, N. J. Olalla, U. Koch, I. Shorubalko, A. Halbritter, and J. Leuthold, Picosecond time-scale resistive switching monitored in real-time, Adv. Electron. Mater. **9**, 2201104 (2023).

[34] T. N. Todorov, J. Hoekstra, and A. P. Sutton, Current-induced forces in atomic-scale conductors, Philos. Mag. B: Phys. Condens. Matter; Statistical Mechanics, Electronic, Optical and Magnetic Properties **80**, 421 (2000).

[35] N. Papior, S. Leitherer, and M. Brandbyge, Simple approach to current-induced bond weakening in ballistic conductors, Phys. Rev. B **106**, 155401 (2022).

[36] T. N. Todorov, Local heating in ballistic atomic-scale contacts, Philos. Mag. B **77**, 965 (1998).

[37] M. Paulsson, T. Frederiksen, and M. Brandbyge, Modeling inelastic phonon scattering in atomic- and molecular-wire junctions, Phys. Rev. B **72**, 201101(R) (2005).

[38] See the Supplemental Material http://link.aps.org/supplemental/10.1103/PhysRevApplied.21.014027 for additional details about the vibrational-pumping model and the simulation, which includes Refs. [43,44].

[39] N. Agraït, C. Untiedt, G. Rubio-Bollinger, and S. Vieira, Onset of energy dissipation in ballistic atomic wires, Phys. Rev. Lett. **88**, 216803 (2002).

[40] H. R. Schober, P. H. Dederichs, K.-H. Hellwege, and J. L. Olsen, *Phonon States of Alloys. Electron States, and Fermi Surfaces of Strained Elements* (Springer-Verlag, Berlin-Heidelberg, 1983).

[41] T. N. Todorov, D. Dundas, A. T. Paxton, and A. P. Horsfield, Nonconservative current-induced forces: A physical interpretation, Beilstein J. Nanotechnol. **2**, 727 (2011).

[42] M. Brandbyge, K. Stokbro, J. Taylor, J.-L. Mozos, and P. Ordejón, Origin of current-induced forces in an atomic gold wire: A first-principles study, Phys. Rev. B **67**, 193104 (2003).

[43] J. G. Kemeny and J. L. Snell, *Finite Markov Chains* (Springer-Verlag, New York-Heidelberg, 1976).

[44] D. Djukic, K. S. Thygesen, C. Untiedt, R. H. M. Smit, K. W. Jacobsen, and J. M. van Ruitenbeek, Stretching dependence of the vibration modes of a single-molecule Pt-H_2-Pt bridge, Phys. Rev. B **71**, 161402 (2005).